QUANTUM DOT AS A MECHANISM TO SUPRESS CHARGE RECOMBINATION IN POLYMER SOLAR CELL

Genene Tessema Mola[a*] and Abiodun Kazeem Ogundele[a]

[a] *School of Chemistry & Physics, University of KwaZulu-Natal, Pietermaritzburg Campus, Private Bag X01, Scottsville 3209, South Africa*

Abstract

Effective light trapping mechanisms in thin film polymer solar cells (PSC) are leveraged by employing group II-VI semiconductor quantum dots. Core-shell semiconductor quantum dots (CdxS/Zn1-xS SQD) were synthesised via the microwave irradiation method. The SQDs were incorporated into the electron transport layer of PTB7:PC71BM blend based polymer solar cell to assist in light trapping and charge collection processes. The experimental findings reported in this study suggest that incorporating SQDs as guest impurities enhances exciton generation, dissociation, energy transfer, and charge collection. Moreover, the performances of the solar cells are found to be dependent on the concentration of SQD in the transport layer. Hence, the best efficiency recorded was 7.13% at an optimal concentration of 0.375 wt.%, which is an increment in PCE by nearly 23%. The SQD acts as conductive fillers, creating improved percolation path that increases conductive networks within the materials. The synergy created by the SQD's inherent features such as quantum confinement effect, carrier multiplication, quantum yields, and photoluminescence phenomena have played important role for the observed changes. These improvements significantly reduce charge recombination during various operational stages of PSCs and improve the shelf life of devices.

Keywords: Quantum Dots, Polymer Solar cell, Solar Energy,

1. Introduction

Solar energy remains one of the cleanest, and most desirable alternative sources of energy to replace those environmentally unfriendly yet depleted fossil fuels to reduce global greenhouse gases (Guo et al., 2023). A vast amount of solar energy, radiated from the Sun per hour could have been enough to fulfil the energy demand for the world population for a year, but unfortunately, it is under-utilized and accounts for only about 4.5% of global electricity generation today, according to the International Energy Agency (IEA). This is due to various reasons ranging from cumbersome manufacturing processes, the high cost of solar cell fabrication, and knowledge gaps on renewable energy sources. Interestingly, organic solar cells (OSC) are cost-effective, lightweight, solution-processable and suitable for roll-to-roll production making them more attractive from an economic perspective with the power conversion efficiencies (PCEs) currently standing over 20%, which is comparable to several to inorganic solar cell technologies (Guo et al., 2023). However, OSCs still suffer from a shortfall in the rate of photon conversion to useful energy because of inherent inadequacies and challenges like environmental instability, low charge transport properties, non-robust temperature tolerance, narrow absorption range, competitive market, facelift cost etc. (Li et al., 2019; Ma et al., 2020).

Various strategies have been employed to improve and advance polymer solar cell technology, enabling it to achieve its full potential as an affordable and cost-effective energy source through roll-to-roll (R2R) production (Oseni & Mola, 2019, Hamed & Mola, 2019). The use of semiconductor quantum dots as guest conductive fillers and impurities in functional layers is an important factor that fits into the third and fourth generations of organic solar cells (Park, K.H. et.al. 2021& Park. S et.al 2021). The use of SQDs in the buffer and interlayers

Selection and/or peer review under responsibility of Scientific Committee
10.18086/eurosun.2024.09.07 Available at http://proceedings.ises.org

is beneficial to the charge transport of polymer solar cells, as reported by different groups. For instance, the incorporation of carbon quantum dots in an electron transport layer (polyethyleneimine ethoxylated) led to enhanced charge extraction (CE) compared with the pristine device without CQD (S. Park et al., 2021) which cumulated in the optimal performance at a 2% concentration of SQD. Another group used conventional architecture to demonstrate the quantum size effects and the crucial role of MoS_2 in extracting holes towards PEDOT:PSS and blocking electrons having been doped in the hole transport layer. The 5nm and 10 nm MoS_2 SQD produced better PV parameters compared to the pristine devices without modified hole transport layers. The 5nm MoS_2 SQD eventually produced optimal PV performance as reported by the group (K. H. Park et al., 2021) traceable to the ability of SQD of that size to capture high photon energy and convert it into useful visible energy. Moreover, the use of SQD in the buffer layer has been reported to delay the degradation of that layer as reported by Lan et al (Lan et al., 2022). The modified device with CdSe@ZnS as the hole extraction layer was found to show a gradual reduction in work function from 4.73 eV to 4.55 eV after 1000 minutes of UV exposures while the pristine device has its work function reduced from 4.86 to 4.25 eV.

In the same vein, the use of bottom-up methods like microwave irradiation method in the synthesis of SQD assists in obtaining high purity and uniformly distributed samples. Other advantages of the microwave irradiation method include reduced environmental hazard, flexibility of materials and compatibility with other materials. The most essential quality of this method is cost-effectiveness, which is consistent with the potential of polymer solar cells. The microwave-irradiation method is fast, easy and scalable.

This study demonstrates the application of microwave-synthesised core-shell semiconductor quantum dot (SQD) ($Cd_xS/Zn_{1-x}S$) in the electron transport layer of an inverted thin film polymer solar cell (TFPSC) containing photo-active layer blends of poly[[4,8–bis[(2-ethylhexyl)oxy]benzo[1,2-b']dithiophene-2,6-diyl][3-fluoro-2-[(2-ethyl hexyl)-carbonyl]thieno [3,4-b]thiophenediyl]]:[6,6]-phenyl C_{71} butyric acid methyl ester (PTB7:PC71BM). The SQD materials ($Cd_xS/Zn_{1-x}S$) with medium energy bandgap core and wide bandgap shell were used in the electron transport layer of TFPSC to assist in improving light trapping in the medium. These combined effects of core-shell SQD can be used to broaden optical absorption spectra leading to high light trapping resulting in improved solar cell performance.

2. Experimental sections

2.1 Synthesis of Semiconductor Quantum Dots

The bottom-up synthesis method involving two precursors was employed here designed by Soltani *et al.*, Shi *et al.*, and Rafea *et al (Rafea et al., 2009; Shi et al., 2011; Soltani et al., 2012)*. The core-shell SQD was synthesised via a two-step path: synthesis of core (Cd_xS) followed by the shell's growth ($Zn_{1-x}S$). 1.33265 g of Cadmium acetate was dissolved in a beaker containing 100 mL of ethylene glycol to obtain 0.05 M, thiol-stabilized with 4 mL thioglycolic acid followed by addition of 0.56343 g (75 mmol) of thioacetamide. The reaction was allowed to stir for about 10 min at about 5000 rpm. The reaction was then transferred into Russel Hobbs (Model no. RHEM21L) domestic microwave with an output power of 700W, the reaction was made to follow a working cycle of 30% for 25 minutes. The second precursor was achieved via the same process with lower concentrations, 0.54873 g (25 mmol) of zinc acetate was dissolved in a beaker containing ethanol, stirred for ten minutes at a speed of 5000 rpm, and later transferred to a microwave oven following a similar working cycle used for the core precursor. The precursors were added dropwise and allowed to disperse uniformly using a sonication bath for 60 min at 40ºC. The final precipitates were cooled to room temperature and centrifuged for about 10 min at a speed of 4000 rpm. This was followed by re-dispersing in deionized water and ethanol several times to remove the excess ionic remnants. Eventually, the SQD was dried in a vacuum oven at 60ºC for 24 h and its morphology was later subjected to various characterisation techniques.

2.2 Devices Fabrication

The un-patterned ITO-coated glass substrates were carefully etched by partially covering the ITO side with photoresist black tape. The uncovered parts of the substrates were then partially immersed in a warm, bubble-

free acidic solution which is made up of hydrochloric acid, nitric acid, and water at the ratio 48%:8%:48%, respectively. The etched substrates were thoroughly and sequentially cleaned with a sonication bath using detergent, deionized water, ethanol, acetone, and isopropanol for 10 min each. The substrates were then blow-dried by a nitrogen gas gun and baked in an oven for 5 min at 100ºC. On the other hand, the polymers blend consisting of PTB7:$PC_{71}BM$ in the ratio 1:1.5 was dissolved in chlorobenzene co-solvent at a concentration of 25 mg/mL and stirred overnight for about 12 h at 30˚C to ensure the miscibility of the polymers. Furthermore, the as-synthesized SQD were dispersed in 0.800 g/mL of zinc oxide nanoparticle ink used as an electron-selective interface layer at different concentrations of 0.125, 0.375 and 0.625 wt.%, respectively. These solutions with different concentrations were stirred for 12 h on a hot plate and were pre-ultrasonicated for 1 h together with the undoped reference solution containing zinc oxide nano ink as indicated in the supplier manual instruction to ensure well-dispersed nanoparticles in the solution. The modified electron selective interface layer solutions were coated on the substrates at 4000 rpm for 40 s, and annealed at 120ºC for 20 min. Then, the photoactive layer was spin-coated from polymers blend solution on all substrates (with precoated modified electron transport layer and reference electron transport layer without SQD) at 1200 rpm for 40 s in an ambient environment and dried inside the furnace for 1 h in a nitrogen-filled atmosphere at a temperature of 50ºC. All samples were later properly mounted on a mask and transferred into the vacuum chamber of the Edward 306 deposition unit, where a 10 nm thin layer of molybdenum trioxide (MoO_3) as the hole transport layer and 80 nm aluminium (Al) as the top electrode was sequentially deposited at a pressure of $1.7 \times 10^{-6}\ mBar$ with an active area of the cells being 2.80 mm^2. The schematic diagram of the device structure and energy level alignment of the materials used are given in Fig.1a. The current density vs. voltage (J-V) characteristics data under illumination and dark conditions were measured using a computer-interfaced Keithley model SS50AAA at a light intensity of 100 $mWcm^{-2}$.

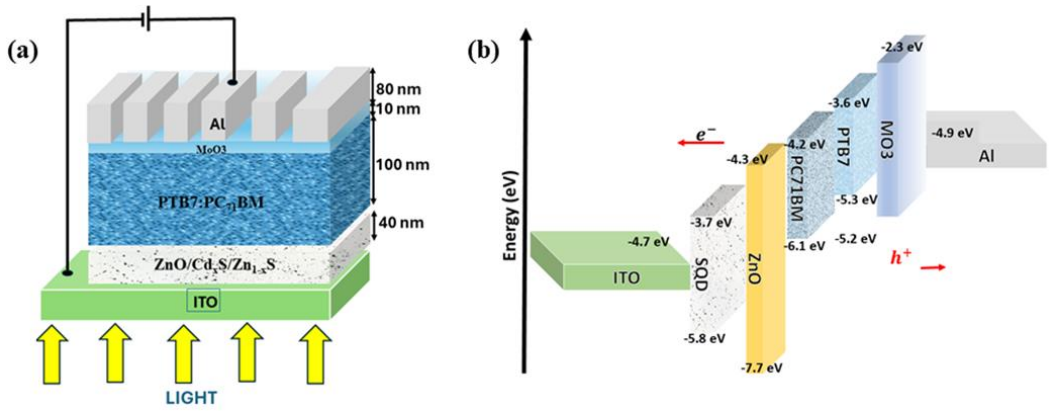

Fig.1: (a) Schematic diagram of device structure (b) Energy level alignments of the materials used

3. Results and discussion

3.1 Morphology of as-synthesized Semiconductor Quantum Dots

The surface morphology of the as-synthesised SQD was studied with a high-resolution tunnelling electron microscope (TEM) and X-ray diffraction (XRD) (see Fig. 2 a & b). The TEM images provided in Fig 2a suggested that the as-synthesized SQD is a core shell. The size distribution observed through the TEM images showed an average of 2.72 nm and 3.67 nm, respectively. On the other hand, the nature of the SQD was further investigated through X-ray diffraction crystallography (Rigaku mini flex) to understand the material crystallographic structure and the crystal phases of the CdS, ZnS and CdS/ZnS SQD (see Fig. 2c). This involves the irradiation of the core-shell SQD with X-rays and the recording of the reflection from different crystal planes. The XRD pattern taken from the samples of SQDs is presented in Fig. 2 b, which clearly showed distinct reflection peak intensities. This is followed by comparing the positions and peaks in the recorded pattern with standard reference patterns in the database. The crystal systems obtained from the JCPD cards (CdS: JCPDS: 8862, ZnS, JCPDS: 3409) show that both the core and shell SQDs are hexagonal with a cell volume of 99.93$Å^3$ (4.1348×3.5810×6.7490) and 156.97 $Å^3$ (3.8140×3.3031×12.4600) respectively.

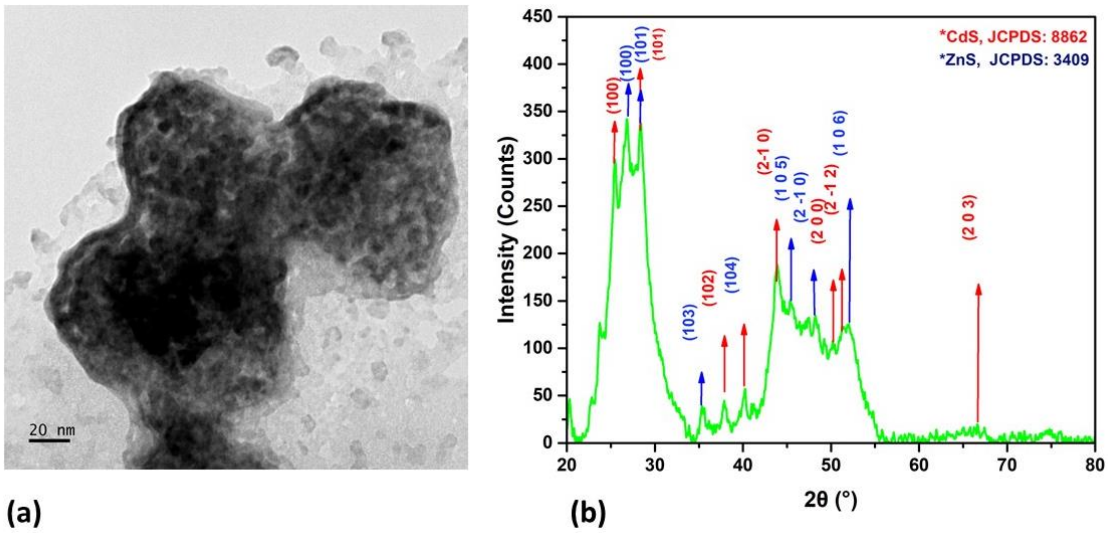

Fig. 2: (a) HRTEM of CdxS/Zn1-xS SQD with its size distribution (b) XRD of the CdxS/Zn1-xS SQD, and (d) EDX of the CdxS/Zn1-xS SQD

The observed peaks at 2θ values are (1 0 0), (1 0 1), (1 0 2), (2-1 0), (2 0 0), (2 -1 2), and (2 0 3) are attributed to CdS core while the peaks at (1 0 0), (101), (103), (104), (105), and (2 -1 0) are attributed to the ZnS shell. At 28.2°, the XRD patterns of CdxS/Zn1-xS SQD revealed a peak overlap at (1 0 1) between the hexagonal structure of core CdS, and the hexagonal structure of ZnS shell. Generally, the well-pronounced sharp peaks, minimal width, and the evaluated narrow size distribution indicate a high crystallinity of the SQD as shown in Fig. 2(a and b) and Table 1. This indicates a favourable electronic state interaction between the core and shell SQD enhancing their performance in PV devices. The elemental analysis of the SQD revealed by energy dispersive X-ray (EDX), indicates the presence of the elements namely cadmium (Cd), zinc (Zn), and sulphur (S) as shown in Fig. 2d. The Scherrer's eq. 1 below was used to obtain crystalline sizes for different peaks.

$$D = k\lambda_{cu}/\beta_{hkl}\cos\theta, \qquad (1)$$

where D is the crystalline size of the SQD, λ_{Cu} is 1.54056 Å (wavelength of copper radiation), k is a constant dependent on the shape of the crystalline material (k= 0.89), β_{hkl} represents the Full Width Half Maximum (FWHM) which is a measure of the difference between two values of the independent variable for which the dependent variable is half of the maximum value, measured in radians, and θ is the Bragg's angle of diffraction in radians. The average size of the XRD was calculated from the data is 3.13 nm. This is also consistent with the values obtained from both TEM images.

3.3 J-V Characteristics of the Devices

An inverted device architecture composed of different layers of materials shown in Fig. 4a is employed in the current investigation. The current density-voltage (J-V) characteristics data under illumination conditions were measured from the fabricated solar cells are provided in Table 2. The data clearly shows an increase in the measured photocurrent as the result of the inclusion of SQD in the charge transport layers at different concentrations (see Fig. 4b & c). Furthermore, the performance of the devices is found to be dependent on the concentration of the SQD in the medium. The best device performance found was PCE = 6.62% at the concentration of 0.375 wt%. This is a growth in PCE by nearly 16% compared to the reference cell. Furthermore, the influence SQD on charge generation/recombination processes was analysed using generated photocurrent (J_{ph}) and effective voltage (V_{eff}) as presented in Fig. 4d to deduce exciton dissociation efficiency, charge collection efficiency, and saturation current (J_{sat}). The latter was used to determine the maximum exciton generation ($G_{max} = {}^{J_{sat}}/_{qL}$). The probabilities of charge dissociation (η_{diss}) and collection (η_{coll}) of the pristine and modified devices were determined by evaluating (${}^{J_{ph}}/_{J_{sat}}$) under short circuit and maximum power output area of the curve, respectively. The device with 0.375 wt.% exhibited the highest

probability of dissociation and collection of charges with the magnitude of 94.71% and 69.9%, respectively as provided in Table 3.

Table 2: The Thin film Polymer solar cells' parameters for devices with/without SQD devices in ETL

$ZnO:/Cd_xS/Zn_{1-x}S$	V_{oc} (V)	$J_{sc}\,(mAcm^{-2})$	FF (%)	PCE (%)	$R_s(\Omega)$	$R_{SH}\,(K\Omega)$
Pristine	0.69 ± 0.01	15.49 ± 0.18	52.59 ± 1.04	5.70 ± 0.08	291.5	8.78
0.125 wt.%	0.63 ± 0.01	17.90 ± 0.93	53.30 ± 1.04	6.62 ± 0.08	234.2	8.68
0.375 wt.%	0.65 ± 0.02	18.95 ± 0.55	54.62 ± 1.62	7.01 ± 0.12	229.2	8.82
0.625 wt.%	0.64 ± 0.04	14.33 ± 0.04	52.00 ± 1.43	4.81 ± 0.08	514.1	10.1

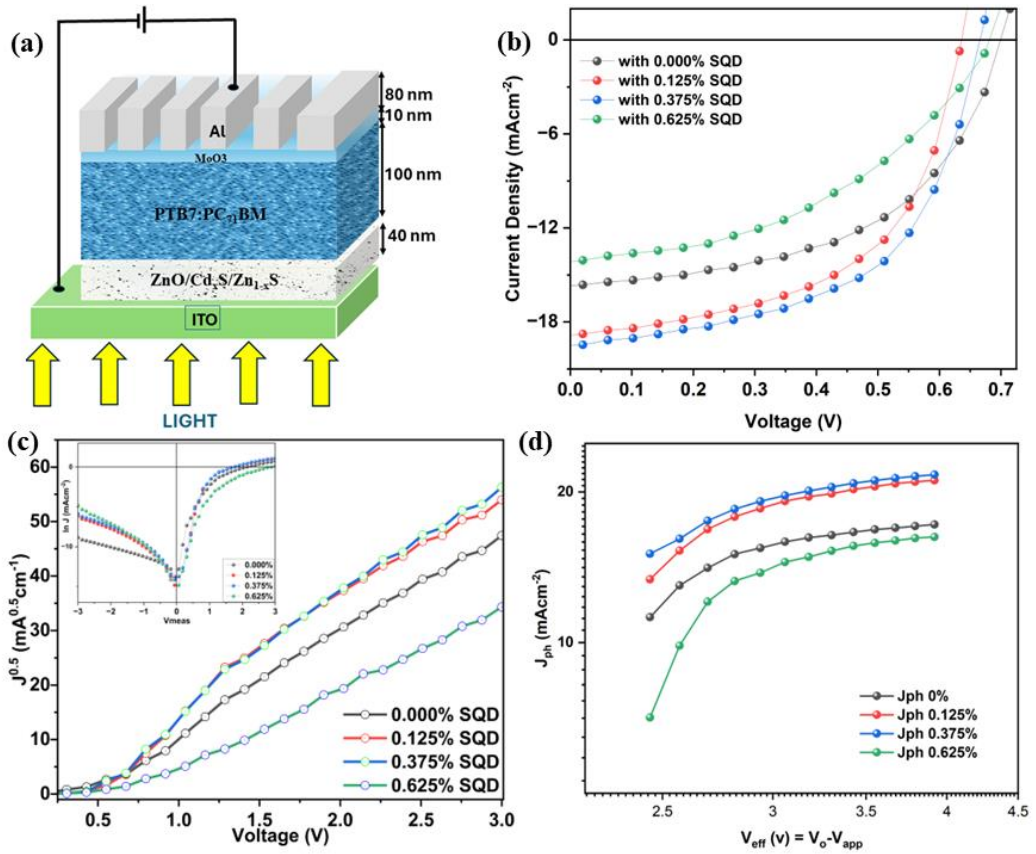

Fig. 4. (a) Inverted device architecture of PSC with modified ETL (b) J-V graphs under illumination & (c) $J^{0.5}$-V graphs under dark conditions (inset SCLC) (d) J_{ph} vs. V_{eff} for TFPSCs pristine and modified ETL devices

Table 3: Charge transport parameters of TFPSCs w/wo SQD in electron transport layer

$ZnO/Cd_xS/Zn_{1-x}S$	$\mu_l(cm^2S^{-1}V^{-1})$	γ (cm V^{-1})	$G_{max}(m^{-3}s^{-1})$	η_{diss} (%)	η_{coll} (%)
Pristine	3.02×10^{-6}	-6.58×10^{-5}	1.08×10^{27}	85.9	66.1
0.125 wt.%	4.12×10^{-6}	-1.76×10^{-4}	1.32×10^{27}	89.3	66.9
0.375 wt.%	4.36×10^{-6}	-1.29×10^{-4}	1.35×10^{27}	94.7	70.0
0.625 wt.%	1.44×10^{-6}	-7.67×10^{-6}	1.02×10^{27}	87.8	62.1

Importantly, all SQD incorporated devices showed enhanced dissociation efficiency, underscoring the positive impacts of the SQD doped into the ETL buffer layer. On the other hand, the impact of SQD on the charge transport processes were investigated using the measured space charge limited current (SCLC) taken without the influence photons generated current. The Mutt-Gurney charge transport equation eq. (2) is used to compare with the SCLC data to be able to derive the transport parameters. The low field mobility (μ_l), which is a measure of charge carriers' movement in the TFPSCs under low electric field conditions and activation factor (γ) can be determined by an equation of the form:

$$J = {}^{9}/_{8}\ \varepsilon_o \varepsilon_r \mu_l\, {V^2}/_{L^3}\, e^{0.89\gamma\sqrt{{V}/{L}}}, \qquad (2)$$

where $\varepsilon_r = 3.5$ is the relative permittivity of PTB7:PC71B, ε_o is the permittivity of free space ($= 8.85 \times 10^{-12}\ m^{-3}kg^{-1}s^4A^2$), L(~ 150 nm) is the distance between the aluminium and ITO electrodes (see Fig 1a). The linear fittings of $J^{0.5}$ against V (obtained under dark conditions) as shown in Fig. 4c were eventually used to determine the values of the low field mobility for pristine devices and SQD-modified

devices. The results of the analysis suggest that indeed the charge mobility in the medium has improved by a factor of 1.4 at the optimum SQD concentration in ETL compared to the reference cell.

4. Conclusion

Core-shell ternary semiconductor quantum dots ($Cd_xS/Zn_{1-x}S$) were employed as a mechanism for light trapping in an inverted TFPSC whose photoactive layer is composed of PTB7:PC71BM blend. The devices with the modified electron transport layer showed significant improvement in power conversion efficiency and device stability compared to the reference cell. The investigation results suggest that the improved device performances depend on SQD concentration in the ETL. The optimum SQD concentration for the best device performance recorded was 0.375 wt.%, which resulted in PCE of 7.01%, which is an increase of 23.4% compared to the reference cell. Such enhanced solar cell performance was attributed to the improved excitons generation, and effective light trapping in the absorber medium. This study showed the characteristic synergy inherent in semiconductor quantum dots in improving the various metrics of thin film polymer solar cells ultimately leading to better device parameters and environmental stability.

5. Acknowledgements

The authors express their profound gratitude for the support from the National Research Foundation (NRF), South Africa and the University of KwaZulu-Natal (UKZN).

6. References

1) Guo, C., Fu, Y., Li, D., Wang, L., Zhou, B., Chen, C., Zhou, J., Sun, Y., Gan, Z., & Liu, D (2023), A polycrystalline polymer donor as pre-aggregate toward ordered molecular aggregation for 19.3% efficiency binary organic solar cells. *Advanced materials*, *35*(41), 2304921.
2) Ian, W., Gu, J., Gao, X., Gong, c., Liu, Y., Zhang, w., Sun, Y., Yue, T., Wei, B., & Zhu, F. (2022), Efficient and ultraviolet-durable nonfullerene organic solar cells: from interfacial passivation and microstructural modification perspectives. *Advanced materials interfaces*, *9*(10), 2101894.
3) Li, K., Wu, Y., Tang, Y., Pan, M. A., Ma, W., Fu, H., Zhan, C., & Yao, J. (2019), Ternary blended fullerene-free polymer solar cells with 16.5% efficiency enabled with a higher-lumo-level acceptor to improve film morphology. A*dvanced energy materials*, *9*(33), 1901728.
4) Ma, Q., Jia, Z., Meng, l., Zhang, J., Zhang, H., Huang, W., Yuan, J., Gao, F., Wan, Y., & Zhang, z. (2020). Promoting charge separation resulting in ternary organic solar cells efficiency over 17.5%. *Nano energy*, *78*, 105272.
5) Oseni, S.O., Mola, G.T. (2019), Bimetallic nanocomposites and the performance of inverted organic solar cell, Composite part B, 172, 660-665

6) Hamed, M.S.G., Mola, G.T. (2019**)**, Copper sulphide as a mechanism to improve energy harvesting in thin film solar cells, Journal of Alloys and Compounds, Vol. 802, 252-258

7) Park, K. H., Jung, S., Kim, J., Ko, B.-M., Shim, W.-G., Hong, S.-G., & Song, S. H. (2021). Boosting photovoltaic performance in organic solar cells by manipulating the size of MoS_2 quantum dots as a hole-transport material. *Nanomaterials*, *11*(6), 1464.
8) Park, S., Lee, H., Park, S. W., Kim, T. E, Park, S. H., Jung, Y. K., & Cho, S. (2021), Improved exciton dissociation efficiency by a carbon-quantum-dot doped workfunction modifying layer in polymer solar cells. *Current applied physics*, *21*, 140-146.
9) Rafea, M. A., Farag, A., & Roushdy, N. (2009). Structural and optical characteristics of nano-sized structure of zn0. 5cd0. 5s thin films prepared by dip-coating method. J*ournal of alloys and compounds*, *485*(1-2), 660-666.
10) Soltani, N., Saion, E., Erfani, M., Bahrami, A., Navaseri, M., Rezaee, K., & Hussein, M. Z. (2012). Facile synthesis of zns/cds and cds/zns core-shell nanoparticles using microwave irradiation and their optical properties. *Chalcogenide Letters*, *9*(9).